

# We are IntechOpen, the world's leading publisher of Open Access books Built by scientists, for scientists

4,800

Open access books available

122,000

International authors and editors

135M

Downloads

Our authors are among the

154

Countries delivered to

TOP 1%

most cited scientists

12.2%

Contributors from top 500 universities



WEB OF SCIENCE™

Selection of our books indexed in the Book Citation Index  
in Web of Science™ Core Collection (BKCI)

Interested in publishing with us?  
Contact [book.department@intechopen.com](mailto:book.department@intechopen.com)

Numbers displayed above are based on latest data collected.  
For more information visit [www.intechopen.com](http://www.intechopen.com)



---

# Interfacial Mechanical Behaviors in Carbon Nanotube

## Assemblies

---

Xiaohua Zhang

Additional information is available at the end of the chapter

<http://dx.doi.org/10.5772/67764>

---

### Abstract

Interface widely exists in carbon nanotube (CNT) assembly materials, taking place at different length scales. It determines severely the mechanical properties of these assembly materials. In this chapter, I assess the mechanical properties of individual CNTs and CNT bundles, the interlayer or intershell mechanics in multiwalled CNTs, the shear properties between adjacent CNTs, and the assembly-dependent mechanical and multifunctional properties of macroscopic CNT fibers and films.

**Keywords:** carbon nanotube, assembly materials, mechanics, interface

---

## 1. Introduction

Carbon nanotubes (CNTs) are hollow cylinders consisting of single or multiple sheets of graphite (graphene) wrapped into a cylinder. After the first observation in 1991 by Iijima [1], extensive work has been carried out to CNTs toward their broad mechanical, electronic, thermal, and optical applications [2, 3]. The fundamental mechanical properties, such as their stiffness, strength, and deformability, have been investigated with extensive theoretical and experimental researches, and been well reviewed, in the past two decades [4–8]. Nowadays, for industrial and engineering applications, CNTs have been assembled into macroscopic materials such as fibers, films, forests, and gels [9–15]. Due to the assembly feature of these materials, the interfacial structure between CNTs always plays a crucial role in determining the tensile or compressive behavior, dynamic response, and coupling phenomenon between

multiple physical properties that take place at the interfaces. Therefore, the utilization efficiency of the mechanical property from individual CNTs to their assembly is a sophisticated function of the assembly structure and types of interfacial interactions.

In this chapter, I will review the mechanics of individual CNTs, discuss the sliding friction between CNTs, and report our recent progresses on the fabrication technique and mechanical properties of macroscopic CNT assembly materials. The general features of the assembly design and interface design will be illustrated from the perspective of interface engineering. The chapter is organized as follows. Section 2 contains a brief description of the mechanical properties of individual CNTs, in terms of modulus, strength, compressibility, and deformability. Section 3 describes the interlayer (intershell) sliding of multiwalled CNTs (MWCNTs) and intertube friction between adjacent CNTs, and the strategies to enhance the interfacial frictions. Section 4 discusses the recent investigations on the interfacial mechanics in macroscopic CNT assembly materials, especially CNT fibers and films where the CNTs are highly aligned or highly entangled. Finally, the chapter concludes with a brief summary and gives an outlook on future developments in the field.

## 2. Mechanical properties of carbon nanotubes

### 2.1. Young's modulus and tensile strength

The basic mechanical properties of CNT are strongly related to the basic properties of a graphene sheet. In these materials, carbon atoms are covalently bonded with three nearest carbon atoms in a hexagonal lattice by forming three  $\sigma$  bonds in the sheet plane and one delocalized  $\pi$ -bond over the basal plane. As the  $sp^2$   $\sigma$  bond is shorter and stronger even than the  $sp^3$  bond in diamond, the axial elastic modulus of CNT and graphene is super high, as expected to be up to several TPa [6, 7]. The first experimental study on the modulus was based on the analysis of thermal vibration of MWCNTs, which showed a wide range of 0.4–4.15 TPa [16]. Later, the modulus was also estimated by the compressive response using micro Raman spectroscopy and was 2.8–3.6 TPa for singlewalled CNTs (SWCNTs) and 1.7–2.4 GPa for MWCNTs [17]. Direct tensile tests showed the modulus ranged from 270 to 950 GPa for individual MWCNTs [18], and from 320 to 1470 GPa when several SWCNTs bundled together as a CNT rope [19]. Besides the experimental evaluations, theoretical estimations also show the similar results. For example, by using an empirical Keating Hamiltonian with parameters determined from first principles, a modulus ranging from 1.5 to 5.0 TPa was estimated [20]. A molecular dynamics (MD) approach showed a modulus of  $\sim 1$  TPa and a shear modulus of  $\sim 0.5$  TPa and predicted that chirality, radius, and number of walls have little effect on the value of Young's modulus [21].

Different from the modulus estimation, measuring the tensile strength of CNTs is a very challenging task. Compared with experiment, it is easier to compute the strength by considering the effects of defects [22, 23], loading rate, temperature [24], and number of walls [25]. Typically, the fraction of CNT involves bond breakage and/or rotation, usually resulting in the formation of specific types of dislocation, such as the pentagon-heptagon (5-7), (5-7-7-5), (5-7-5-8-5) defects [26]. MD simulations showed that CNT under tension behaves as a brittle

material at high strain (15%) and low temperature (1300 K), or as a ductile material at low strain (3%) and high temperature (3000 K) [26–28]. Such tensile behaviors depend on the evolution of the dislocation. For example, the (5-7-7-5) dislocation can either separate into two (5-7) pairs to result in a ductile transformation or involve into a crack to result in a brittle fracture. An alternative pathway for the fracture of CNT was also proposed by the direct bond-breaking through the formation of a series of virtual defects at high tensions [23]. These studies were usually based on the consideration of the formation of energy for the dislocations. However, another MD study showed that the fracture behavior is almost independent of the separation energy and to depend primarily on the inflection point in the interatomic potential [22]. The fracture strength should be moderately dependent on tube chirality, and the strength and fracture strain were estimated to be 93.5–112 GPa and 15.8–18.7%, respectively. **Figure 1a** shows two different stress-strain curves for a (20,0) CNT, where the modified Morse potentials with interatomic force peaks at 19 and 13% strain were used. To show the effect of structural defect, a result for a missing atom is provided where the strength was reduced by about 25%.

The tensile strength and the fracture of CNT were also measured directly with experiment [18, 19]. The measurement of 19 MWCNTs showed a strength of 11–63 GPa and a strain at break up to 12% [18]. The failure of MWCNTs was described in term of the “sword-in-sheath” type fracture, where the outermost shell broke first followed by the pull out of the rest of the shells from the outermost shell. When SWCNTs were bundled to be a rope, the tensile strength was measured to be 13–52 GPa, based on 15 measurements, and the strain at break was up to 5.3%, see **Figure 1b** [19]. The stretchability of CNT was also experimentally obtained by deforming freely suspended SWCNT ropes, where the maximum strain was up to  $5.8 \pm 0.9\%$  [29]. By measuring the stress-induced fragmentation of MWCNTs in a polymer matrix, the tube strength was up to 55 GPa [30]. Another pulling and bending tests on individual CNTs in-situ in a transition electron microscope (TEM) showed a tensile strength of  $\sim 150$  GPa, suggesting that the strength is a large fraction of the elastic modulus [31].

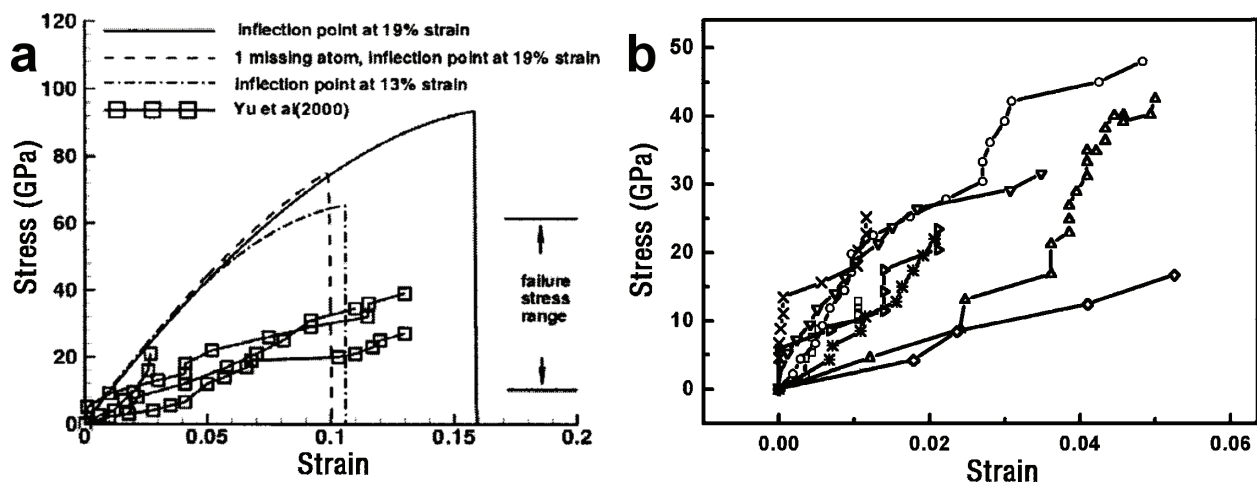


**Figure 1.** (a) A strong dependence on the inflection point in the interatomic potential can be seen from the stress-strain curves for a (20,0) CNT, and a missing atom has also a significant effect on strength, reducing it by about 25% [22]. Experimental measurements on MWCNTs are provided for comparison [18]. (b) Eight stress-strain curves obtained from the tensile-loading experiments on SWCNT ropes [19].

## 2.2. Compressibility and deformability

Different from the high rigidity and high strength along the axial direction, CNT is relatively compressible and deformable in the transverse direction. When individual SWCNTs are bundled together, significant deformation could occur by van der Waals (vdW) interaction between the adjacent tubes [32]. Fully collapsed MWCNTs were first observed with TEM [33]. Large diameter CNTs could also form the partial and full collapse on substrate [34–36]. The structural deformation can be induced by applying pressure. Various experiments on SWCNT bundles have shown clear evidence of structural deformation or transition [37–42]. MD simulations revealed that the compressibility and deformability are dependent on the tube diameter and the number of walls [43]. By applying a certain high pressure, there could be a circular-to-elliptical shape transition of the tube's cross section for either individual CNTs or their bundles [44–51]. These structural deformations are all reversible upon unloading the pressure. In a different way, a very large force exerted on CNT could still produce reversible and elastic deformation, and that radial mechanical forces might not be capable of cutting a CNT [43]. By examining the ballistic impact and bouncing-back processes, large diameter CNTs could withstand high bullet speeds [52].

Upon compressing, bending, or twisting, structural deformations of CNT become more complicated. With an increasing compression stress, different buckling patterns in CNT at the point of instabilities can be created [53]. As shown in **Figure 2**, each shape change corresponds

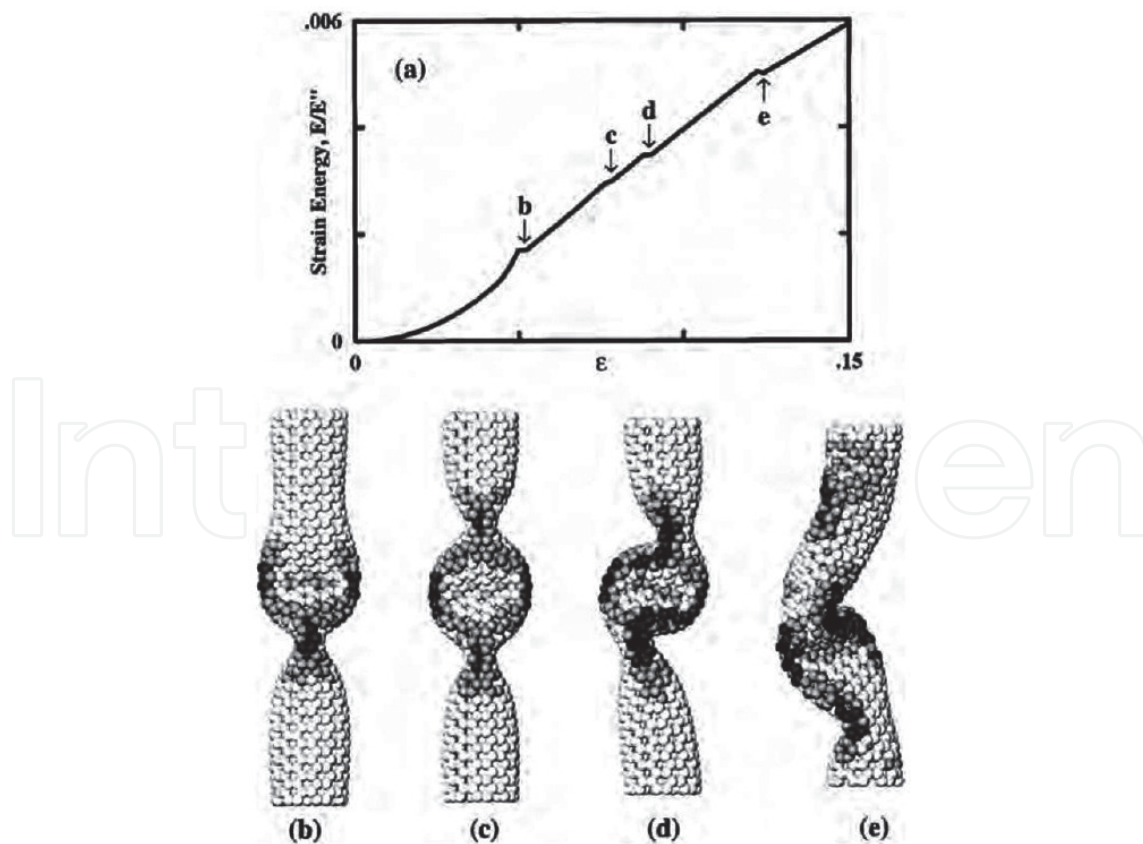


**Figure 2.** The strain energy (a) displays four singularities corresponding to shape changes (b–e) with increasing the axial compression [53].



to an abrupt release of energy and a singularity in the stress-strain curve. MD simulations showed that the presence of intertube vdW interactions tends to weaken the CNT bundles under compression [55]. On the other hand, with increasing the tube diameter, the bending modulus was found to decrease sharply [56], as a rippling mode becomes energetically favorable [57, 58]. The modeling on the wavelike distortion indicated that there is a critical diameter at a given load and a CNT length, for the emergence of the rippling mode [59]. It was also found that thick MWCNTs are very prone to develop rippling deformations in bending and twisting, governed by the interplay of strain energy relaxation and intertube interactions [58, 60]. **Figure 3** shows experimental observations of partially collapsed segments in freestanding and twisted MWCNTs with TEM [54].

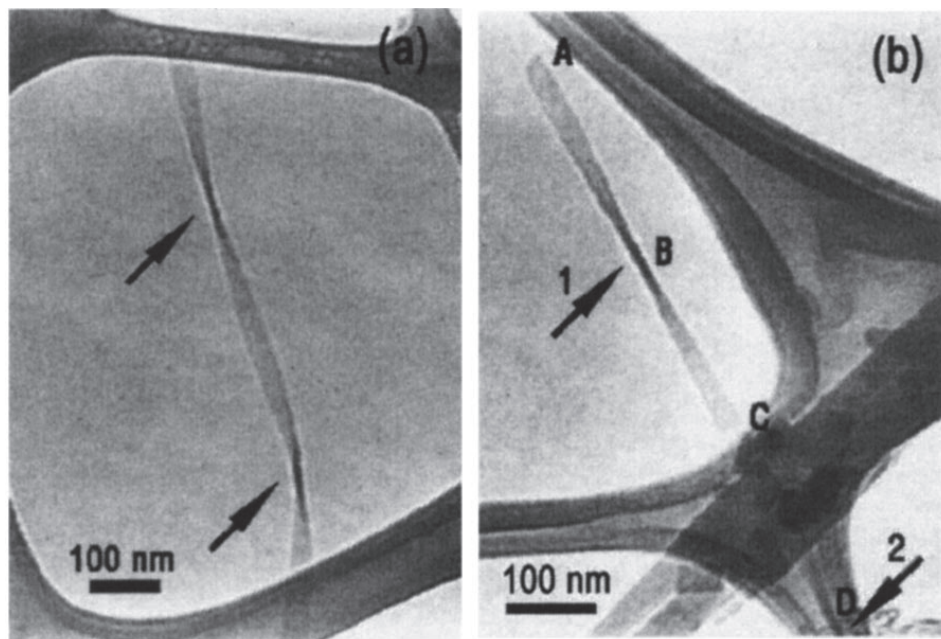


**Figure 3.** TEM images showing a suspended, fully collapsed, and twisted MWCNT (a), and a freestanding, fully collapsed, and twisted MWCNT (b) on a lacy carbon TEM grid [7, 54].

### 3. Interlayer and intertube interactions

#### 3.1. Sliding between MWCNT shells

Different from SWCNTs, the interlayer interactions in MWCNTs exhibit interesting sliding phenomena during the tensile stretching and self-oscillation. By modeling of the interlayer interaction with different atomic potentials, such as the classic Lennard-Jones (LJ) potential and the registry-dependent Kolmogorov-Crespi (KC) potential (zeroth generation RDP0 [61] and first generation RPD1 [62]), could cause significantly different energy corrugation between graphitic layers [62–65]. Nevertheless, the interlayer sliding has been systematically studied despite the type of atomic potential. Experiments have also shown the interlayer sliding and superlubricity of CNTs.

Experimental measurements on the dependence of the sliding force against the contact length between the MWCNT shells suggested several responsible sources including the surface tension, the shear elastic force, and the edge (tube termination) effect force [66]. The shear strength was found to be 0.08–0.3 MPa depending on the interlayer commensurability. After the inner shells were pulled out from the outer shells, spontaneous retraction was observed with TEM due to the attractive vdW forces between these shells [67]. The interlayer static and dynamic shear strengths were estimated to be 0.43–0.66 MPa. The telescoping motion of an MWCNT also showed an ultralow friction, below  $1.4 \times 10^{-15}$  N per atom ( $8.7 \times 10^{-4}$  meV  $\text{\AA}^{-1}$ ) [68]. More direct observation of the superlubricity in doublewalled CNTs (DWCNTs) was conducted by extracting the inner shell out from a centimeters-long DWCNT, where the inner-shell friction (vdW force) was estimated to be 1.37–1.64 nN (the total number of atoms was unknown, yet could be over  $10^8$ – $10^9$  for a tube length of 1 cm) [69], corresponding to a friction force of about  $10^{-6}$ – $10^{-5}$  meV  $\text{\AA}^{-1}$  per atom. By following the low-friction induced telescoping, gigahertz oscillators were theoretically proposed based on the oscillatory extrusion and retraction of the inner shells [70–77], and the interlayer commensurability determines the rate of energy dissipation during the oscillation [71]. The friction force between oscillatory layers was estimated to range from  $10^{-17}$  to  $10^{-14}$  N per atom, about  $6 \times 10^{-6}$ – $0.006$  meV  $\text{\AA}^{-1}$  [73]. Similarly, the rotation between CNT shells and the rotational friction was observed or measured by experiments and simulations [78–81]. The rotational friction is a broadband phenomenon, as it does not depend strongly on a specific vibrational mode but rather appears to occur from the aggregate interactions of many modes at different frequencies [82].

At high sliding speeds, the friction between CNT layers was not hydrodynamical, in fact not even monotonic with the sliding speed [83]. A high speed can develop a sharp friction peak and onset parametric excitation of CNT's "breathing" phonon modes. **Figure 4a** shows that there is

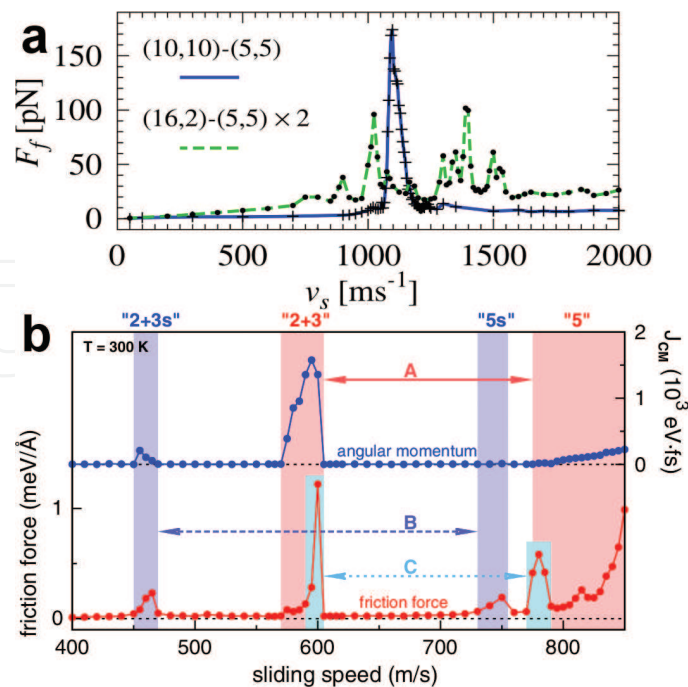


**Figure 4.** (a) There is a massive increase in friction at  $\sim 1100$   $\text{m s}^{-1}$  for the (5,5)@(10,10) DWCNT [83]. (b) The center-of-mass angular momentum  $J_{\text{CM}}$  (top) and the sliding frictional force per inner tube atom (bottom) as functions of the sliding speed [84]. A, B, and C are three resonance regions related the giant friction forces.

a massive increase in sliding friction at a speed of  $\sim 1100 \text{ m s}^{-1}$  for a (5,5)@(10,10) DWCNT. The highest friction force could be up to 170 pN, corresponding to  $\sim 0.15 \text{ meV \AA}^{-1}$  per inner tube atom. The main source of the interlayer friction was believed to be the inner nanotube terminations [85], while the “bulk” friction was unfortunately considered to be irrelevant.

To understand the “bulk” frictional behavior, two groups of studies were carried out [65, 84, 86]; pulling simulations where a constant external force was applied on each atom of the inner tube along the tube axis, and rigid sliding simulations where the inner tube was constrained to slide as a whole at a fixed speed. The pulling simulation revealed a static friction (depinning) force of  $0.02 \text{ meV \AA}^{-1}$  at 300 K and  $0.1 \text{ meV \AA}^{-1}$  at 50 K for the (5,5)@(10,10) DWCNT. After the depinning, the speed of the inner tube jumps directly to plateaus. Three speed plateaus are seen at  $v \approx 450, 720,$  and  $780 \text{ m s}^{-1}$ . This phenomenon is ubiquitous as it is also observed for an incommensurate case where a chiral (11,2) tube slides inside a (12,12). The general occurrence of plateaus and jumps is a natural consequence of frictional peaks for growing the speed. **Figure 4b** shows sharp frictional peaks near  $v \approx 450, 570, 720,$  and an important threshold onset near  $780 \text{ m s}^{-1}$ . These peaks are known to generally arise out of parametric excitation of the “breathing” phonon modes, classified by an angular momentum index  $n$  (for tangential quantization around the tube axis). Such nonmonotonic force-speed characteristics imply a “negative differential friction,” whereby an increasing applied force yields an inner tube sliding speed that grows by jumps and plateaus, rather than smoothly.

The surprise comes from analyzing the two parts of angular momentum  $J = J_{\text{CM}} + J_{\text{pseudo}}$  around the tube axis such as its center-of-mass (rigid body rotation with angular velocity  $\omega$ ) and shape-rotation (“pseudorotational”) parts [65, 84]. Generally, zero at generic sliding speed due to lack of nanotube chirality,  $J_{\text{pseudo}} = -J_{\text{CM}} = 0$ ,  $J_{\text{pseudo}}$  jumps to nonzero values at the frictional peaks and past the threshold, where  $J_{\text{pseudo}} = -J_{\text{CM}} / \neq 0$ , see **Figure 4b**. This is a spontaneous breaking of chiral symmetry occurring in nanoscale friction, whose mechanism is from the third- and fourth-order energy nonlinearities. The inner-tube sliding causes a washboard frequency due to the lattice periodicity  $a_{\text{CC}} = 2.46 \text{ \AA}$ . At the critical frequencies, the ‘ $n = 5'$ ’ or ‘ $2 + 3 = 5'$ ’ excitations are observed, where the DWCNT’s  $n = 5$  mode is resonantly excited or the  $n = 2, 3, 5$  modes are jointly excited by the simple matching condition  $2 + 3 = 5$ . Besides these “normal” excitations (labeled A in **Figure 4b**), there are ‘ $n = 5s'$ ’ and ‘ $2 + 3s = 5'$ ’ excitations, where the  $3s$  and  $5s$  are the single outer tube’s phonon modes. These excitations are labeled B in **Figure 4b**. The two C-peaks in **Figure 4b** are ascribed to the phenomenon of strong stick-slip frictions, possibly related to the phonon modes along the tube axis.

### 3.2. Intertube friction

In most of the cases, individual CNTs are bundled together as a CNT rope, owing to the strong aggregation tendency between adjacent CNTs. As mentioned above, experimental measurement showed a tensile strength just up to 13–52 GPa [19], far below the ideal strength for individual CNTs. The easy sliding between adjacent CNTs has become a severe problem hindering their engineering applications. For example, slip rather than breakage of individual CNTs was observed in the fracture test of polymers reinforced by CNT bundles [87]. As CNTs can contact with each other in parallel way or at certain cross angles, the interfacial shear strengths between CNTs should be discussed separately.



The static and kinetic frictions between two perpendicular CNTs were investigated experimentally. A coefficient of friction of  $0.006 \pm 0.003$  was obtained by sliding an MWCNT perpendicularly on a SWCNT surface, and the shear strength was derived to be  $4 \pm 1$  MPa [88]. The shear strength was one to two orders of magnitude larger than the intershell shear strength of 0.05 MPa for MWCNTs in vacuum, possibly due to the presence of water at the intertube interface in ambient. A following experiment, namely a vertical friction loop measurement, was proposed to characterize the adhesion and friction properties between CNTs [89]. An MWCNT tip was ramped in the vertical direction against a suspended SWCNT. During ramping, a stick-slip motion was found to dominate the sliding, attributed to the presence of defect-induced or amorphous-carbon-associated high energy points on the tip surface. Surprisingly, the coefficients of static friction and shear strength were finally evaluated to be about 0.2 and 1.4 GPa, respectively.

MD simulations showed that the sliding behaviors and interfacial shear strengths between two crossly contacting CNTs are much more complicated than the frictions between CNTs and graphite, graphite and graphite, and the inner and outer shells of MWCNTs [90]. The simulation was performed on two SWCNTs in contact at different cross angles. For the parallel contact, the axial interfacial shear strengths between the zigzag-zigzag ( $\sim 0.25$  GPa) and armchair-armchair pairs ( $\sim 0.5$  GPa) are two orders of magnitude larger than those of CNTs having different chiralities (0.5–1 MPa). CNTs with diameters larger than 1 nm will slide relatively from an AB stacking position to the next nearest AB stacking position while smaller ones do not slide through AB stacking positions. For two cross contacting CNTs, the magnitude of interfacial shear strength is much less dependent upon tube chirality. The highest value of shear strength was reported to be about 1 GPa in SWCNT bundles, however, still as quite low as to be improved for applications in high-performance composite materials [91].

### 3.3. Strategies to improve the intertube load transfer

A molecular mechanics modeling showed that in order to make the strength of a CNT bundle as high as that of the lowest value of individual CNTs (11 GPa), the contact length should be up to  $\sim 3800$  nm, by assuming the CNTs are bundled together without changing their circular cross sections [63]. With considering the vdW-force-induced radial deformation [32], the intertube distance-of-closest changes from 3.34 to 3.25 Å for (10,10) CNT bundles, the required contact distance for 11 GPa can decrease to  $\sim 1300$  nm. This implies that the key to improve the intertube load transfer is the interface design between CNTs.

Twist is an effective way to induce strong radial deformation for CNT bundles. **Figure 5a** shows the cross sections obtained from MD simulations with increasing the twist level and **Figure 5b** shows the corresponding transferred load due to the shape deformation at twist angles of 0, 30, 60, 90, 120, 150, 180, and 210° [63]. It was observed that the individual CNTs start to collapse in the cross section, and therefore, more atoms are in close contact. For the case of no twist, a force of only  $\sim 0.048$  eV Å<sup>-1</sup> is transferred to the center tube, while at 120° the transferred load increases to 1.63 eV Å<sup>-1</sup>. Clearly, the radial deformation strongly depends on the twist angle, which consequently changes the nature of the contact and contributes to a new interlayer tribology.

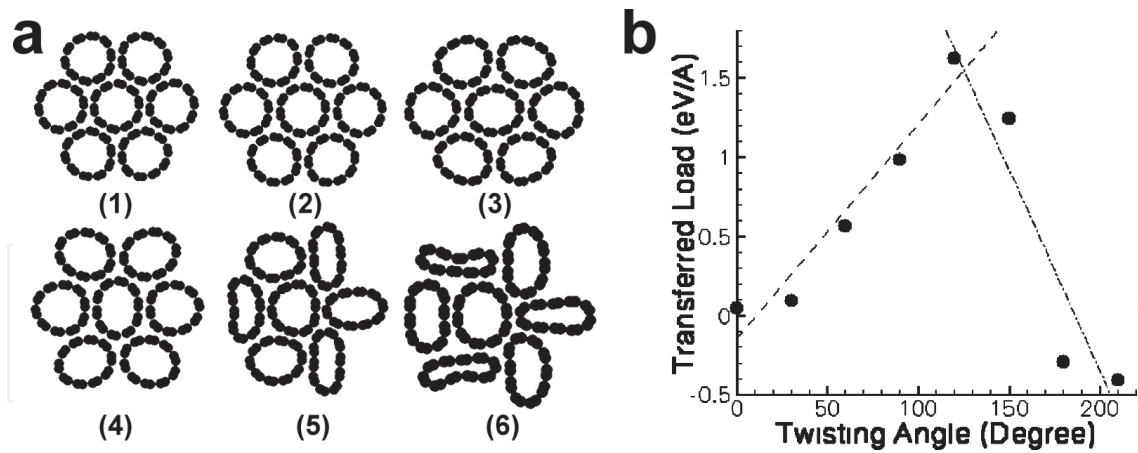


**Figure 5.** (a) Change in cross section at the mid-length of a SWCNT bundle with increasing the twist level and (b) the corresponding load transfer ability as a function of twist angle [63].

Even a slight structural deformation could cause an improved load transfer. For example, when a DWCNT was slightly bent into a curved one, the energy transfer between the two tubes becomes much faster than that between two straight tubes [81]. Slight displacement of the inner tube could add a large degree of disturbance to the DWCNT's original state of equilibrium and thus present strong inertia to oppose the extraction process, indicating the importance of the inner tube as structural support for the outer tube [92].

Pressure-induced structural phase transition could be a new strategy to improve the intertube load transfer [51]. For a CNT bundle containing 16 (23,0) SWCNTs, the intertube static friction can be improve from  $0.1 \text{ eV } \text{Å}^{-1}$  per atom to  $0.4\text{--}0.45 \text{ eV } \text{Å}^{-1}$  after all the tubes collapse under pressure higher than 0.5 GPa, see **Figure 6**. Due to the large tube diameter, the collapsed CNT structure

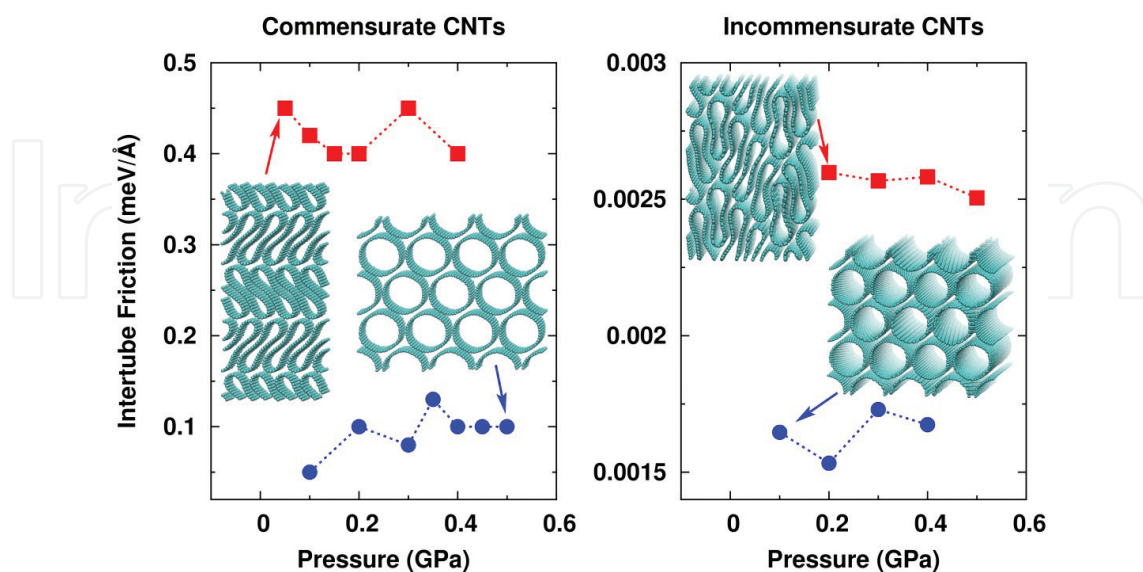


**Figure 6.** The intertube friction force can be increased by a factor of 1.5–4, depending on tube chirality and radius, when all tubes collapse above a critical pressure and when the bundle remains collapsed with unloading down to atmospheric pressure [51].

can be well maintained even by unloading the pressure down to 0.05 GPa. In order to realize a 10 GPa tensile strength, the minimum tube length should be just 167 nm, much smaller than the length of 1090 nm before the phase transition. For a CNT bundle containing totally different tube chiralities, the dynamic friction force can be improved from 0.0017 to 0.0026 eV Å<sup>-1</sup> after the phase transition. Such study also indicated that fewwalled large-diameter CNTs could be very important for engineering applications due to the easy ability to induce the collapse phase transition.

Covalent bonding between the shells in MWCNTs or between adjacent CNTs can increase the interlayer and intertube shear strength by several orders of magnitude [93–95]. The covalent intershell bonds can be formed due to the on-shell vacancies or intershell interstitials. According to the types of defect, the force needed to initiate sliding of the shells varies from 0.08 to 0.4 nN for a single vacancy to 3.8–7.8 nN for two vacancies, an intershell interstitial, and an intershell dimer [93]. Therefore, small-dose electron or ion irradiations are suggested to partially transfer the load to the nanotube inner shells. MD simulations revealed that interwall sp<sup>3</sup> bonds and interstitial carbon atoms can increase load transfer between DWCNT walls and that interwall sp<sup>3</sup> bonds are the most effective [95]. Similarly, by using moderate electron-beam irradiation inside a TEM, stable links between adjacent CNTs within bundles were covalently formed [94]. At a high irradiation energy of 200 keV, there was a substantial increase in effective bending modulus and thus an increase in shear modulus for low doses, while a long irradiation time rather damaged the well-ordered structure of tubes (**Figure 7**). At 80 keV, electrons were shown not to damage isolated CNTs but had enough energy to lead to the formation

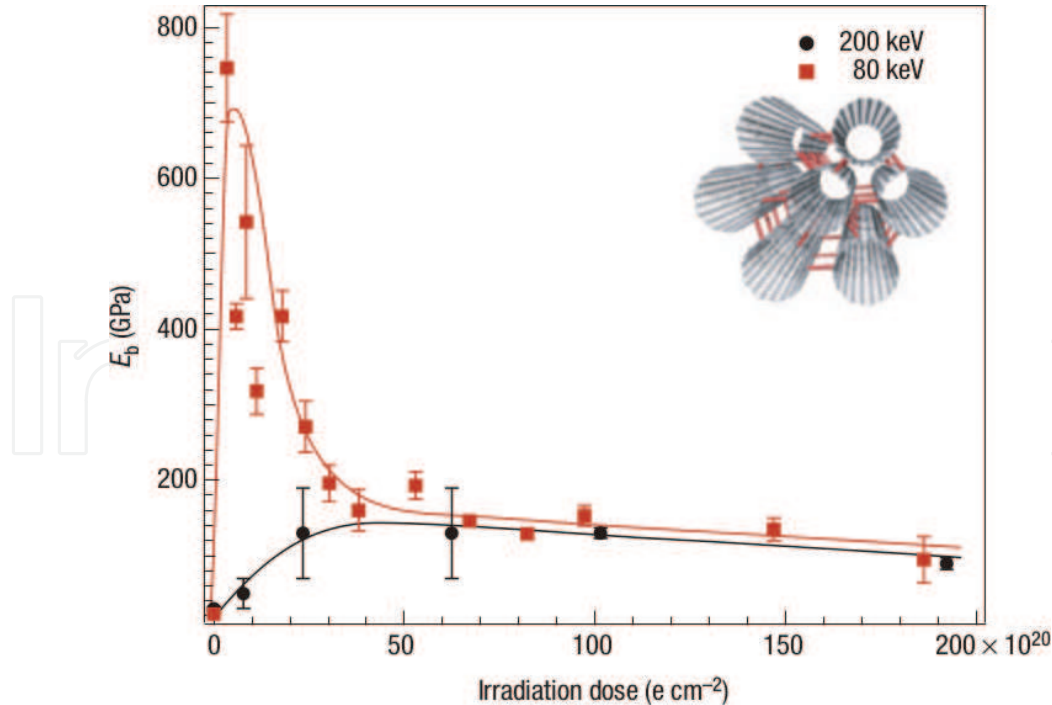


**Figure 7.** Behavior of bending modulus as a function of received dose for two incident electron energies [94]. For 200 keV, the modulus increases on short exposures, due to cross-linking and degrades at higher exposures because of structural damage. The bundle irradiated with 80-keV electrons shows a much stronger and sharper increase of the bending modulus.

of mobile interstitial atoms in the confined space between adjacent CNTs. As a result of the newly formed covalent bonds, a huge increase of the bending modulus by a factor of thirty was observed (**Figure 7**). However, a long-time dose at low energies could still cause the accumulation of damage to the structure, making the mechanical performance to decrease eventually.

Even without introducing covalent bonding between the  $sp^2$  layers, the existence of structural defects in either CNT layer could lead to a sharp increase in friction and energy dissipation rate [64].

However, besides the tube structure, defect level, and intertube contact, there are many other issues in macroscopic CNT assembly materials. For example, the CNT packing density, alignment, entanglement, aggregation size, and surface functionalization could be important structural parameters, as to be discussed below.

## 4. Carbon nanotube assembly materials

So far, CNT fibers, films, forests, and gels are well-known and typical macroscopic assembly materials where the CNTs are the main constituents, especially at a mass fraction much more than 50% [10]. For example, CNT fiber is a one-dimensional assembly containing millions of individual tubes [9, 11–13, 15]. It has been found that CNT fibers could have much higher specific modulus and specific strength than those of commercial carbon and polymeric fibers. For the composite materials, there have been two different applications of CNTs such as a dispersion-based fabrication by using CNTs as reinforcing fillers in a polymer matrix [96, 97] and an assembly-based fabrication by directly assembling CNTs into composites [14]. In the former, the CNT content is strongly limited to be no larger than ~5 wt%, while in the latter, a small amount of polymer molecules (about 20–30 wt%) are used to strengthen the interfaces between CNTs. To describe these macroscopic CNT materials, different structural parameters are proposed and investigated in the past decade.

### 4.1. CNT fibers

CNT fiber can be produced by the coagulation-based “wet spinning” [98–101], the “direct spinning” from a CNT aerogel [102–104] or similarly from a pre-formed CNT film [105], and the “forest spinning” based on vertically aligned CNT forests [106–108]. A CNT fiber with a diameter of ~10  $\mu\text{m}$  usually contains more than  $10^6$  individual CNTs. Such assembly feature is different from those well-known fibers for many years, which are usually a solid structure without internal interfaces. CNT fiber can also be considered a continuous length of interlocked “filaments” (CNT bundles), where the bundles are formed during the CNT growth rather than in the spinning process. As I have pointed out recently [109], although also being called as CNT yarn, CNT fiber is indeed not a yarn because the CNT bundles are not macroscopically processable. On the contrary, the basic components of a yarn, the long and parallel or interlocked filaments, are usually processable objects with a width larger than several micrometers [110].



Twist is the most fundamental treatment to make the CNTs assembled into a continuous fiber with a circular cross section. The as-spun fiber is relatively loose with noticeable spaces between CNTs or CNT bundles when the twist angle is small. Increasing the twist angle is an effective method to densify CNT fibers and thus improves the friction coefficient between the CNTs. **Figure 8** shows the strength-twist relationship for different CNT fibers [111–113]. All studies showed that the highest fiber strength was found at a twist angle of 15–20°. However, with further increasing the twist, the load (upon stretching) compresses the fiber rather than acts totally along the fiber axis due to the twist angle between the CNTs and the axis, making the utilization efficiency to decrease at high twist angles. The experimental observations that the strength initially increases with twist angle and then decreases are almost the same as those in traditional textile yarns. Nevertheless, the constituent CNTs are different from the filaments in a textile yarn; the CNTs are hollow cylinders and can deform the cross section under pressure due to a structural phase transition [44–49]. For those fibers spun from few-walled CNTs (wall numbers smaller than 6), it can be seen that beyond the optimal twist angle, an additional strength peak is at large twist angle of 27–30°. This second peak arises from the collapse transformation of the CNT hollow structure, which renders the CNT bundles much stronger and reduces the bundle cross-sectional area.

Solvent densification is another interfacial treatment to CNT assemblies, due to a large capillary force [114, 115]. Therefore, liquid infiltration by using water, ethanol, acetone, or dimethyl sulfoxide (DMSO) is also often used in the method of array spinning to densify CNT fibers [116–119]. Although the densification process does not improve nanotube orientation, it enhances the load transfer between the nanotubes, thus ensuring that most of them are fully load-bearing. For example, the fiber diameter was shrunk from 11.5 to 9.7  $\mu\text{m}$  after acetone shrinking [117]. However, the role of solvent is hardly known as the capillary force can be influenced by the solvents volatility (boiling point), surface tension, and interaction with CNT surfaces. By comparing various solvents including the nonpolar solvents of *n*-hexane, cyclohexane, cyclohexene, toluene, and styrene, polar protic solvents of glycerine, methanol, ethanol, water, ethylene glycol, and 1,3-propanediol, and polar aprotic solvents of

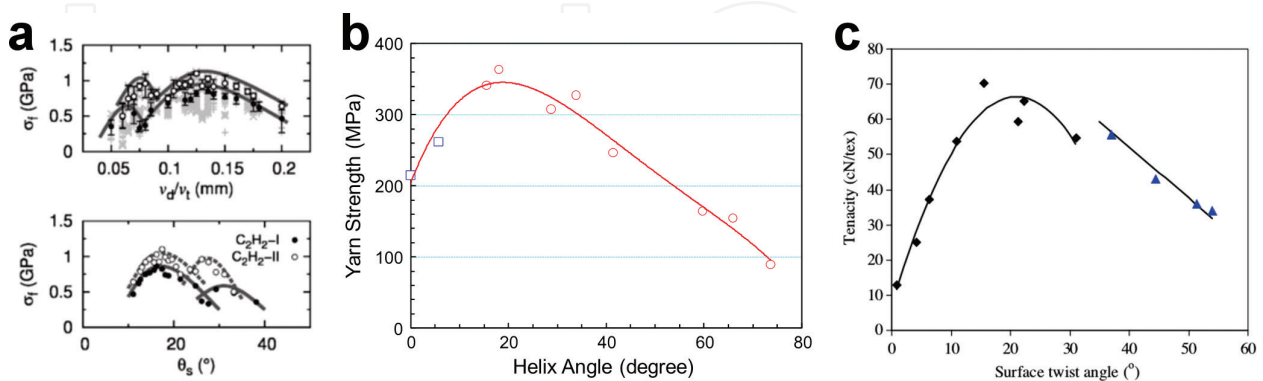


**Figure 8.** (a) Double-peak strength behavior of CNT fibers with increasing twist angles [111]. The surface twist angle ( $\theta_s$ ) depends on the twisting and drawing speeds ( $v_t$  and  $v_d$ ) by  $\theta_s = \arccos \{ (v_d/v_t) / [(\pi d_t)^2 + (v_d/v_t)^2]^{1/2} \}$ , where  $d_t$  is the fiber diameter and is  $>10.5 \mu\text{m}$ . (b) Dependence of yarn tensile strength on helix angle for forest-spun MWCNT fibers [112]. The fiber diameter was  $\sim 20 \mu\text{m}$ . (c) Relationship between the fiber's specific strength and tenacity with the surface twist angle [113].



ethyl acetate, acetone, acetonitrile, *N,N*-dimethylformamide (DMF), DMSO, and *N*-methyl-2-pyrrolidone (NMP), only few highly polar solvents show high densifying ability to CNTs, namely DMF, DMSO, NMP, and ethylene glycol, despite of their high boiling points and low evaporation rates [118]. These solvents increased the fiber strength from 864 MPa (dry-spun) or 1.19 GPa (ethanol) to 1.14–1.35 GPa (DMF, DMSO, NMP) or 1.33–1.58 GPa (ethylene glycol). Clearly, the solvent polarity shows a key role in determining the capillary, as the polarity induced attractive binding energy with CNT ( $E_{\text{ind}}$ ) goes up quadratically with the solvent's local dipole moment  $\mu$ , by  $E_{\text{ind}} = -\mu^2\alpha/(4\pi\epsilon_0)^2r^6$ , where  $\alpha$  is the static polarizability of CNT,  $\epsilon_0$  is the vacuum permittivity, and  $r$  is the distance between the dipole moment and the CNT surface [120, 121].

In addition to twisting and liquid densification, polymer impregnation is another effective treatment to enhance the mechanical properties of CNT fibers. The polymers are introduced to bridge nonneighboring CNTs, such as polyethyleneimine (PEI) [122], polydopamine (PDA) [123], polyvinyl alcohol (PVA) [105, 118, 124], polyacrylate [125], polyvinylidene fluoride (PVDF) [126], epoxy [105], polyimide (PI) [118, 127], and bismaleimide (BMI) [118, 128]. **Figure 9** shows several typical stress-strain curves for polymer-reinforced CNT fibers, such as PI, BMI, PEI, and PDA [118, 122, 123]. The enhanced mechanical properties of CNT fibers with polymer impregnation are attributed to couplings between the CNT network and polymer chains occurring at the molecular level. As a result, the sliding between CNTs can be remarkably hindered by the polymer network, especially that formed by the cured thermosetting polymers. Therefore, more external strain can be transferred to the CNTs as shown in **Figure 10**, where the Raman peaks of CNTs downshift to a lower wavenumber by different values under axial strains [105]. Both PVA and epoxy enhanced the downshifts, corresponding to the improved load transfer between CNTs. The cured thermosetting polymer network also shows advantages in improving the fiber modulus, as indicated by the largest change in  $G'$ -peak wavelength. Similarly, PI and BMI are other efficient thermosetting polymers for producing high-modulus CNT fibers [118, 127, 128]. However, other polymers might be good at improving the fiber's stretchability and toughness by preventing the sliding-induced fiber fracture, possibly due to the polymer wrapping around the CNT connections [126], cooperative deformation mechanisms of the soft and hard segments [125], iron-mediated covalent cross-linking [122], or cross-linked polymeric binders [123].

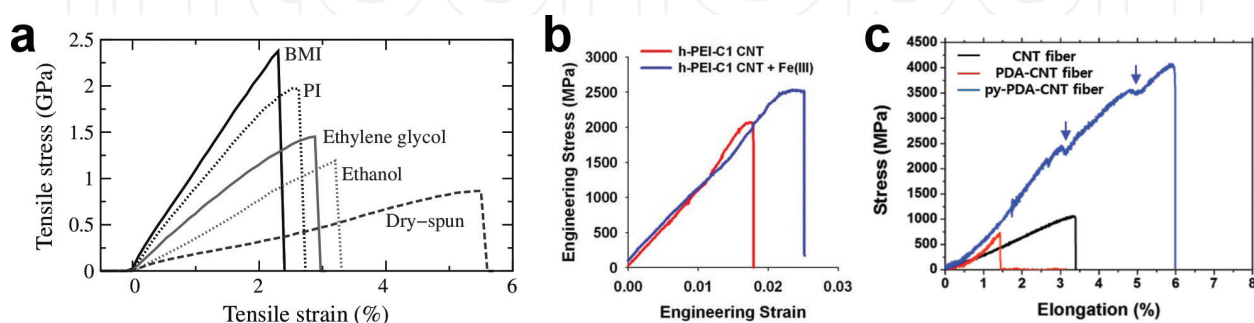


**Figure 9.** (a) Stress-strain curves of dry-spun, ethanol-densified, ethylene-glycol-densified, PI-reinforced, and BMI-reinforced CNT fibers [118]. (b) Stress-strain curves of PEI-catechol-reinforced CNT fibers, including one after addition of Fe(III) [122]. (c) Stress-strain curves of as-drawn CNT fiber, CNT/PDA fiber, and CNT/(pyrolyzed PDA) fiber [123].

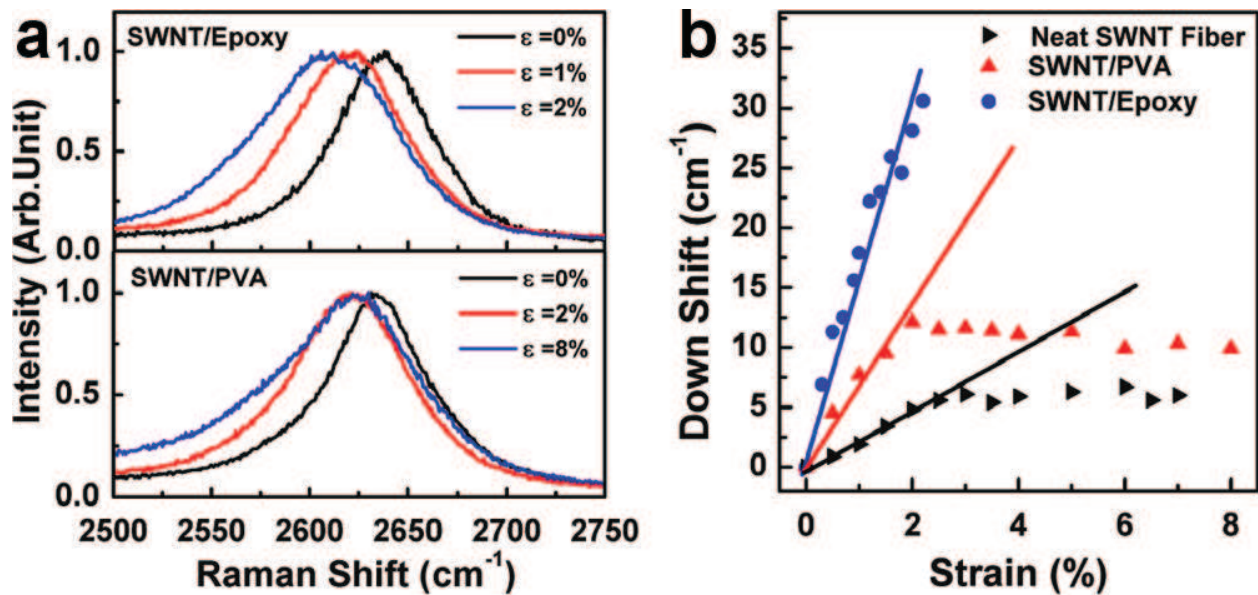


Figure 10. Variations of Raman spectra under strain in different systems [105]. (a) Typical  $G'$  band Raman spectra of epoxy- and PVA-infiltrated CNT fibers. (b) Downshifts of the peak position in different systems.

The structure of CNT fiber is hierarchical, with CNTs self-assembling into bundles and the bundles forming an aligned network in the fiber [129, 130]. Other assembly parameters also include the tube waviness or straightness [131], which can also result in different elasticity and modulus for CNT fibers. Notice that the above-mechanical improvements are irrelevant to the microstructure of individual CNTs but are relevant to the macroscopic assembly parameters. From the point of view of tube structure, fewwalled CNTs have shown advantages in producing high-performance fibers, rather than the ideal SWCNTs [131]. For the SWCNTs, usually 1–1.5 nm in diameter, simulations and experiments have shown that a certain high pressure (hundreds of MPa) is necessary to introduce even a slight deformation of their cross sections. That means, the intertube contact area is far limited compared with the overall circumference of the cross section. While for the fewwalled tubes, the tube diameter can be large up to  $\geq 5$  nm, making it much easy to deform the cross section and increase the contact area. Experiments even have shown, upon certain twisting and/or tensioning, collapse of fewwalled tubes were possibly introduced [111, 132].

Furthermore, covalent interface engineering could be an efficient posttreatment for the as-produced CNT fibers. Acid treatment could introduce rich hydroxyl, methyl/methylene, and carbonyl groups onto CNT surfaces, which also made CNT fibers shrunk slightly, or more densified. Such treatment enhanced the load transfer between CNTs, according to a theoretical study [94], and thus resulted in an increase in fiber strength and modulus [133]. Recently, by using an incandescent tension annealing process (ITAP), where the current-induced Joule heating increase the temperature of CNT fiber up to 2000°C in vacuum,  $sp^3$  covalent bonding was observed in CNT fibers [134]. As a result, the fiber modulus could be improved from 37 to 170 GPa, once the ITAP was performed with maintaining a high tension on the fiber.

In order to further improve the utilization efficiency of the individual CNT's mechanical properties in CNT fibers, more effort should be paid to the delicate combining of the choice

of CNT structure, controlling in CNT packing density, alignment, and straightness, and inter-tube mechanics engineering by polymers or covalent functionalization.

## 4.2. CNT films

CNT films are another important macroscopic material with high mechanical performances. Various processing methods have been developed to produce CNT films by using preformed CNT assemblies, among which these two methods are of great importance: the layer-by-layer stacking of aligned CNT sheets and the stretching on entangled CNT webs [14]. Despite of the fabrication methods, there are also many common problems concerning with the interface mechanics, as the CNT fibers do.

For instance, liquid densification is widely used to CNT films [135–137], and polymer impregnation can remarkably improve the interfacial load transfer [138–143]. Different from CNT fibers where the tubes are assembled with the aid of twisting, there is more freedom to tune the assembly structure. The CNTs can be got superaligned by stretching the films in a wet environment [135], or by microcombing before they are layer-by-layer stacked [136]. After improving the CNT alignment, the pure CNT films could be as strong as 3.2 GPa in tensile strength, with a Young’s modulus of 124–172 GPa [135, 136]. **Figure 11** shows the stress-strain curves for the CNT films being both densified and superaligned. Once these aligned CNTs were impregnated with polymers, especially thermosetting polymers, the film’s strength and modulus could be further improved. At a mass fraction of 50–55% for CNT, the CNT/BMI composite films exhibited a strength of 3.8 GPa and a modulus of 293 GPa [139]. Such superior properties are derived from the long length, high mass fraction, good alignment, and reduced waviness of the CNTs.

The stretching on entangled CNT webs is another way to obtain highly aligned CNT films. With the aid of BMI impregnation and curing, the strength and modulus of the CNT/BMI composite films could be improved from 620 MPa and 47 GPa (un-stretched) to 1600 MPa and

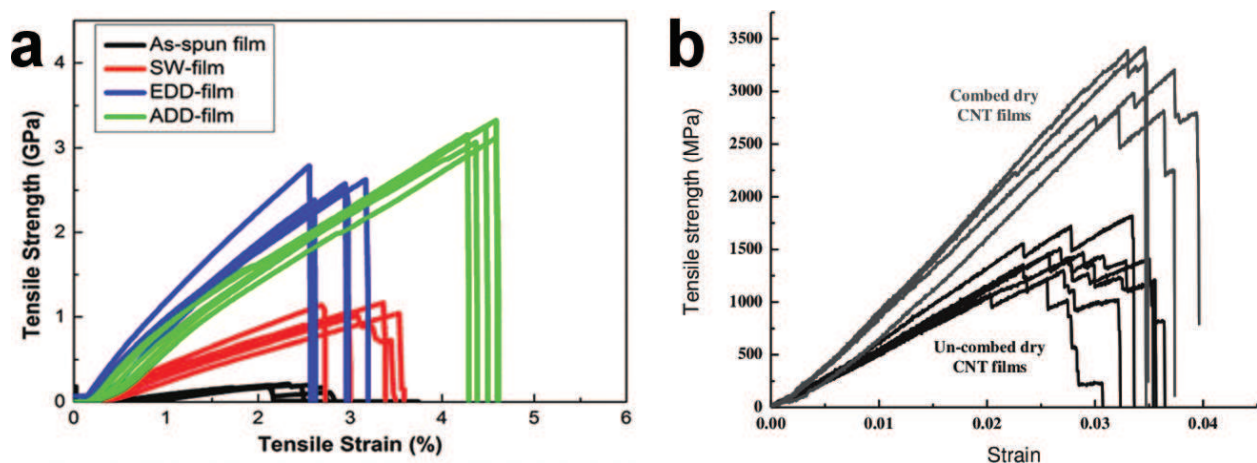


**Figure 11.** Stress-strain curves for CNT films obtained by a stretch-dip-drying method (a) [135] and a microcombing method (b) [136]. The films treated with acetone (ADD) and ethanol (EDD) were much stronger than the as-spun and spray-wound (SW) films. The films after microcombing had a larger Young’s modulus than the ADD and EDD films.



122 GPa, 1800 MPa and 150 GPa, and 2088 MPa and 169 GPa after being stretched by 30, 35, and 40%, respectively [140]. By further introducing surface functionalization for CNTs, the strength and modulus were surprisingly improved up to 3081 MPa and 350 GPa, respectively [141].

However, the direct stacking of CNT sheets and stretching on CNT webs could not avoid the CNT aggregation due to the vdW interactions. As shown in **Figure 12a** and **b**, the aggregation size was up to hundreds of nanometer [143]. Such aggregation of nanometer-sized components has become a severe problem in paving the way to stronger materials [144]. In the aggregation phase, the intertube load transfer is not as efficient as at the CNT-polymer interface. Thus, such aggregation phase becomes the weak parts in the composites and hinders further reinforcement. In an ideal structure, the nanometer-sized components should be uniformly distributed in the matrix without forming any aggregation phases. Therefore, all the interfaces can play roles in shear load transfer. As inspired by the formation process of natural composite structures, the BMI resins were infiltrated into CNT webs before any stretching was performed. Since the liquid treatment just densifies the CNT network without inducing CNT aggregation, the impregnation before stretching causes each CNT or CNT bundle uniformly covered by a thin layer of polymers. Therefore, the following stretching could just align the CNTs but avoid the aggregation due to the thin layer of polymer, resulting in an optimized composite structure. By adapting a multistep stretching process, the final

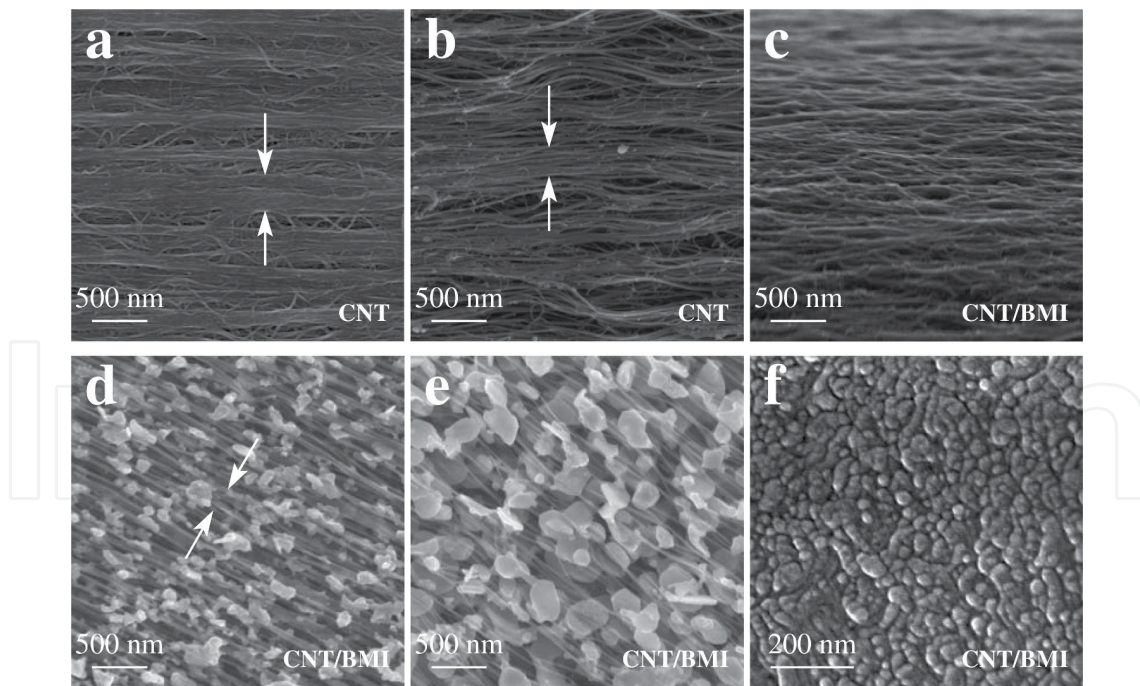


**Figure 12.** Comparison of CNT assembly structure for different films [143]. (a,b) CNT aggregation in the layer-by-layer stacking of array-drawn CNT sheets and the stretched dry films composed by entangled CNTs, respectively. (c) The small-sized CNT bundles did not aggregate but were surrounded by BMI polymers and uniformly distributed. (d, e) 750°C treated CNT/BMI composite films where the stretching was performed before and after resin impregnation, respectively, showing the aggregation and unaggregation. (f) Cross section of the optimal CNT/BMI composite structure by using focused ion beam treatment, indicating an aggregation size of 20–50 nm for the CNTs.

composite film exhibited superior mechanical performances. The highest tensile strength and modulus were up to 5.77–6.94 and 212–351 GPa at a CNT-to-resin mass ratio of 7:3 and a stretching magnitude of 34% [143].

**Figure 12c** shows the morphology of the optimized CNT/BMI composites, where the CNT bundles were found to be uniformly distributed and aligned. To characterize the aggregation of CNTs, thermal treatment and focused ion beam treatment were used. After being heated to 750°C to decompose the polymers, the remaining CNTs were found to be aggregated/unaggregated if the stretching was performed before/after the polymer impregnation, see **Figure 12d** and **e**. The direct observation of the cross section with focused ion beam treatment showed an aggregation size of just 20–50 nm (**Figure 12f**), a size for the bundling that was still difficult to avoid during the growth process.

On the whole, for the macroscopic CNT assemblies, the interface mechanics becomes much more complicated as the material exhibits a collective dynamics from the constituent CNTs. Assembly parameters, including CNT packing density, alignment and/or entanglement, twisting level, cross-linking, and aggregation size, are found to be critical for the mechanical properties. By controlling the interface mechanics in the CNT assemblies, we can not only optimize the mechanical properties, but also introduce multifunctionalities, as discussed below.

### 4.3. Multifunctionalization by interface engineering

Besides load transfer at the intertube interfaces, energy dissipation is also a common interfacial phenomenon. As CNT fiber is formed by assembling millions of individual tubes, the assembly features provide the fiber with rich interface structures and various ways of energy dissipation, including the internal viscosity and intertube friction [109]. Therefore, a modified Kelvin-Voigt model was adopted, where an elastic spring  $K$ , a viscous damping coefficient  $\eta$ , and an intertube friction  $f$  are connected in parallel [145]. Due to the friction, there exists a friction-dependent component in loss tangent, which is not dependent on the frequency. As shown in **Figure 13**, the loss tangent was nonzero (about 0.045) for the dry-spun CNT fibers, while that for the T300 carbon fiber was nearly zero due to the absence of interfaces. When the CNT fibers were densified

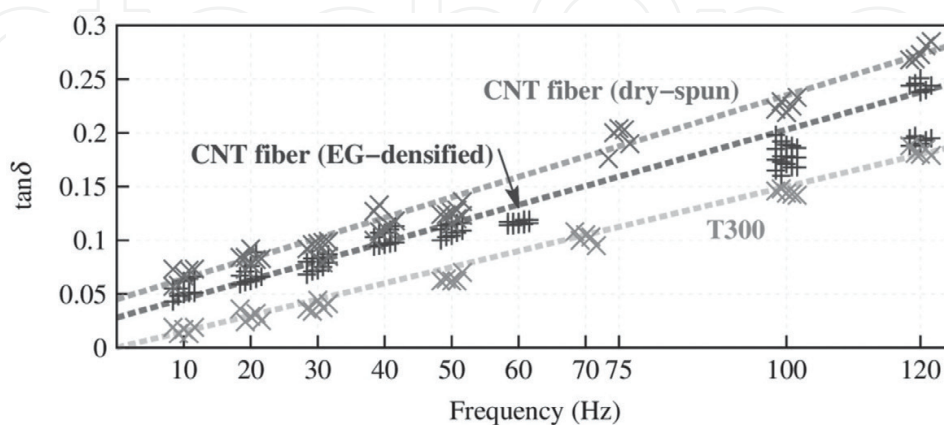


**Figure 13.** The frequency dependence of loss tangent for the dry-spun CNT fiber, ethylene-glycol-densified CNT fiber, and T300 carbon fiber [109].



by ethylene glycol, the CNTs became constrained, corresponding to reduced loss tangents, see **Figure 13**. Based on the friction-based Kelvin-Voigt model, the damping performance of CNT fibers can be tuned in a very wide range. The introduction of thermosetting polymers further decreases the loss tangent, while plying CNT fibers into a yarn increases the loss tangent [109].

The CNT entanglement provides another way to enhance the damping ability [146]. The as-produced CNT films based on an injection chemical vapor deposition exhibited a loss tangent of 0.37–0.42 at 200 Hz [146], or 0.2 at 50 Hz [143]. After the network was stretched and strengthened with BMI, the loss tangent could decrease remarkably down to about 0.05 at 50 Hz [143].

When an electric current is passing through CNT assemblies, there exist parallel currents along the aligned CNTs. The collective electromagnetic force between parallel current can cause a volume contraction for the assembly [147]. Based on such mechanism, CNT fibers can be developed as electromechanical actuator. Detailed study revealed that the electromechanical coupling is quite complicated beyond the actuation [128]. For example, when a current passes through a CNT fiber, the fiber's modulus could decrease remarkably due to the current-induced weakening in C–C  $\sigma$  bond. Besides the electromechanical coupling, the current could induce a strong Joule heating, making the fiber temperature to increase very sharply. Such electrothermal coupling can be used for fast curing to the impregnated thermosetting resins at a moderate temperature of 200–300°C [128], or for the formation of intertube  $sp^3$  covalent bonding at a high temperature of 2000°C in vacuum [134].

## 5. Conclusion

The control of interface mechanics is a key strategy to develop high-performance CNT assembly structures. High tensile properties (strength up to 3–6 GPa and modulus up to 200–350 GPa) can be obtained for aligned CNT fibers and films, corresponding to an improved utilization efficiency of CNT's mechanical properties. Furthermore, the dynamical performance and multifunctionalities both depend strongly on the interface between CNTs, also in terms of CNT packing density, alignment, entanglement, twisting level, cross-linking, and aggregation size. For future development of high-performance CNT assembly materials, more delicate design on the multiscale interfaces is required. I hope this review could cast lights for the interface design ranging widely from the nanometer scale to the macroscopic scale.

## Acknowledgements

The author thanks Prof. Xingao Gong of Fudan University, Prof. Erio Tosatti of the International School for Advanced Studies, and Prof. Qingwen Li of Suzhou Institute of Nano-Tech and Nano-Bionics for their kind collaborations, which are the important sources for this chapter. Financial supports from the National Natural Science Foundation of China (11302241, 51561145008), Youth Innovation Promotion Association of the Chinese Academy of Sciences (2015256), and National Key Research and Development Program of China (2016YFA0203301) are acknowledged.

## Author details

Xiaohua Zhang

Address all correspondence to: [zhangxhcm@gmail.com](mailto:zhangxhcm@gmail.com)

1 Suzhou Institute of Nano-Tech and Nano-Bionics, Chinese Academy of Sciences, Suzhou, China

2 Jiangsu Key Laboratory of Engineering Mechanics and Department of Engineering Mechanics, School of Civil Engineering, Southeast University, Nanjing, China

## References

- [1] Iijima S. Helical microtubules of graphitic carbon. *Nature*. 1991;**354**(6348):56–58
- [2] Baughman RH, Zakhidov AA, De Heer WA. Carbon nanotubes—the route toward applications. *Science*. 2002;**297**(5582):787–792
- [3] De Volder MFL, Tawfick SH, Baughman RH, Hart AJ. Carbon nanotubes: present and future commercial applications. *Science*. 2013;**339**(6119):535–539
- [4] Qian D, Wagner GJ, Liu WK, Yu M-F, Ruoff RS. Mechanics of carbon nanotubes. *Applied Mechanics Reviews*. 2002;**55**(6):495–533
- [5] Bernholc J, Brenner D, Nardelli MB, Meunier V, Roland C. Mechanical and electrical properties of nanotubes. *Annual Review of Materials Research*. 2002;**32**:347–375
- [6] Ruoff RS, Qian D, Liu WK. Mechanical properties of carbon nanotubes: theoretical predictions and experimental measurements. *Comptes Rendus Physique*. 2003;**4**(9):993–1008
- [7] Yu M-F. Fundamental mechanical properties of carbon nanotubes: current understanding and the related experimental studies. *Journal of Engineering Materials and Technology*. 2004;**126**(3):271–278
- [8] Kis A, Zettl A. Nanomechanics of carbon nanotubes. *Philosophical Transactions of the Royal Society London A*. 2008;**366**(1870):1591–1611
- [9] Behabtu N, Green MJ, Pasquali M. Carbon nanotube-based neat fibers. *Nano Today*. 2008;**3**(5–6):24–34
- [10] Liu L, Ma W, Zhang Z. Macroscopic carbon nanotube assemblies: preparation, properties, and potential applications. *Small*. 2011;**7**(11):1504–1520
- [11] Zhang X, Li Q. Toward multifunctional carbon nanotube fibers. In: Q. Zhang, editor. *Carbon Nanotubes and Their Applications*. Singapore: Pan Stanford Publishing; 2012. pp. 467–499. Chapter 14
- [12] Lu W, Zu M, Byun J-H, Kim B-S, Chou T-W. State of the art of carbon nanotube fibers: opportunities and challenges. *Advanced Materials*. 2012;**24**(14):1805–1833

- [13] Miao M. Yarn spun from carbon nanotube forests: production, structure, properties and applications. *Particuology*. 2013;**11**(4):378–393
- [14] Zhang X, Yu X, Zhao J, Li Q. Bio-inspired design and fabrication of super-strong and multifunctional carbon nanotube composites. In: Berber MR, Hafez IH, editors. *Carbon Nanotubes - Current Progress of Their Polymer Composites*. Rijeka, Croatia: InTech - Open Access; 2016. pp. 73–93. Chapter 3
- [15] Di J, Zhang X, Yong Z, Zhang Y, Li D, Li R, Li Q. Carbon-nanotube fibers for wearable devices and smart textiles. *Advanced Materials*. 2016;**28**(47):10529–10538
- [16] Treacy MMJ, Ebbesen TW, Gibson JM. Exceptionally high Young's modulus observed for individual carbon nanotubes. *Nature*. 1996;**381**(6584):678–680
- [17] Lourie O, Wagner HD. Evaluation of Young's modulus of carbon nanotubes by Micro-Raman spectroscopy. *Journal of Materials Research*. 1998;**13**(9):2418–2422
- [18] Yu M-F, Lourie O, Dyer MJ, Moloni K, Kelly TF, Ruoff RS. Strength and breaking mechanism of multiwalled carbon nanotubes under tensile load. *Science*. 2000;**287**(5453):637–640
- [19] Yu M-F, Files BS, Arepalli S, Ruoff RS. Tensile loading of ropes of single wall carbon nanotubes and their mechanical properties. *Physical Review Letters*. 2000;**84**(24):5552–5555
- [20] Overney G, Zhong W, Tománek D. Structural rigidity and low frequency vibrational modes of long carbon tubules. *Zeitschrift fur Physik D*. 1993;**27**(1):93–96
- [21] Lu JP. Elastic properties of carbon nanotubes and nanoropes. *Physical Review Letters*. 1997;**79**(7):1297–1300
- [22] Belytschko T, Xiao SP, Schatz GC, Ruoff RS. Atomistic simulations of nanotube fracture. *Physical Review B*. 2002;**65**(23):235430
- [23] Dumitrică T, Belytschko T, Yakobson BI. Bond-breaking bifurcation states in carbon nanotube fracture. *Journal of Chemical Physics*. 2003;**118**(21):9485–9488
- [24] Wei C, Cho K, Srivastava D. Tensile strength of carbon nanotubes under realistic temperature and strain rate. *Physical Review B*. 2003;**67**(11):115407
- [25] Liew KM, Wong CH, He XQ, Tan MJ, Meguid SA. Nanomechanics of single and multi-walled carbon nanotubes. *Physical Review B*. 2004;**69**(11):115429
- [26] Bernholc J, Brabec C, Nardelli MB, Maiti A, Roland C, Yakobson BI. Theory of growth and mechanical properties of nanotubes. *Applied Physics A*. 1998;**67**(1):39–46
- [27] Nardelli MB, Yakobson BI, Bernholc J. Brittle and ductile behavior in carbon nanotubes. *Physical Review Letters*. 1998;**81**(21):4656–4659
- [28] Nardelli MB, Yakobson BI, Bernholc J. Mechanism of strain release in carbon nanotubes. *Physical Review B*. 1998;**57**(8):R4277–4280

- [29] Walters DA, Ericson LM, Casavant MJ, Liu J, Colbert DT, Smith KA, Smalley RE. Elastic strain of freely suspended single-wall carbon nanotube ropes. *Applied Physics Letters*. 1999;**74**(25):3803–3085
- [30] Wagner HD, Lourie O, Feldman Y, Tenne R. Stress-induced fragmentation of multiwall carbon nanotubes in a polymer matrix. *Applied Physics Letters*. 1998;**72**(2):188–189
- [31] Demczyk BG, Wang YM, Cumings J, Hetman M, Han W, Zettl A, Ritchie RO. Direct mechanical measurement of the tensile strength and elastic modulus of multiwalled carbon nanotubes. *Materials Science and Engineering A*. 2002;**334**(1–2):173–198
- [32] Tersoff J, Ruoff RS. Structural properties of a carbon-nanotube crystal. *Physical Review Letters*. 1994;**73**(5):676–679
- [33] Chopra NG, Benedict LX, Crespi VH, Cohen ML, Louie SG, Zettl A. Fully collapsed carbon nanotubes. *Nature*. 1995;**377**(6545):135–138
- [34] Hertel T, Martel R, Avouris P. Manipulation of individual carbon nanotubes and their interaction with surfaces. *Journal of Physical Chemistry B*. 1998;**102**(6):910–915
- [35] Hertel T, Walkup RE, Avouris P. Deformation of carbon nanotubes by surface van der Waals forces. *Physical Review B*. 1998;**58**(20):13870–13873
- [36] Yu M-F, Kowalewski T, Ruoff RS. Structural analysis of collapsed, and twisted and collapsed, multiwalled carbon nanotubes by atomic force microscopy. *Physical Review Letters*. 2001;**86**(1):87–90
- [37] Chesnokov SA, Nalimova VA, Rinzler AG, Smalley RE, Fischer JE. Mechanical energy storage in carbon nanotube springs. *Physical Review Letters*. 1999;**82**(2):343–346
- [38] Venkateswaran UD, Rao AM, Richter E, Menon M, Rinzler A, Smalley RE, Eklund PC. Probing the single-wall carbon nanotube bundle: Raman scattering under high pressure. *Physical Review B*. 1999;**59**(16):10928–10934
- [39] Peters MJ, McNeil LE, Lu JP, Kahn D. Structural phase transition in carbon nanotube bundles under pressure. *Physical Review B*. 2000;**61**(9):5939–5944
- [40] Gaál R, Salvétat J-P, Forró L. Pressure dependence of the resistivity of single-wall carbon nanotube ropes. *Physical Review B*. 2000;**61**(11):7320–7323
- [41] Tang J, Qin L-C, Sasaki T, Yudasaka M, Matsushita A, Iijima S. Compressibility and polygonization of single-walled carbon nanotubes under hydrostatic pressure. *Physical Review Letters*. 2000;**85**(9):1887–1889
- [42] López MJ, Rubio A, Alonso JA, Qin L-C, Iijima S. Novel polygonized single-wall carbon nanotube bundles. *Physical Review Letters*. 2001;**86**(14):3056–3059
- [43] Lordi V, Yao N. Radial compression and controlled cutting of carbon nanotubes. *Journal of Chemical Physics*. 1998;**109**(6):2509–2512

- [44] Elliott JA, Sandler JKW, Windle AH, Young RJ, Shaffer MSP. Collapse of single-wall carbon nanotubes is diameter dependent. *Physical Review Letters*. 2004;**92**(9):095501
- [45] Zhang XH, Sun DY, Liu ZF, Gong XG. Structure and phase transitions of single-wall carbon nanotube bundles under hydrostatic pressure. *Physical Review B*. 2004;**70**(3):035422
- [46] Zhang XH, Liu ZF, Gong XG. Comment on collapse of single-wall carbon nanotubes is diameter dependent. *Physical Review Letters*. 2004;**93**(14):149601
- [47] Sun DY, Shu DJ, Ji M, Liu F, Wang M, Gong XG. Pressure-induced hard-to-soft transition of a single carbon nanotube. *Physical Review B*. 2004;**70**(16):165417
- [48] Ye X, Sun DY, Gong XG. Pressure-induced structural transition of double-walled carbon nanotubes. *Physical Review B*. 2005;**72**(3):035454
- [49] Gadagkar V, Maiti PK, Lansac Y, Jagota A, Sood AK. Collapse of double-walled carbon nanotube bundles under hydrostatic pressure. *Physical Review B*. 2006;**73**(8):085402
- [50] Chang T. Dominoes in carbon nanotubes. *Physical Review Letters*. 2008;**101**(17):175501
- [51] Zhang X, Li Q. Enhancement of friction between carbon nanotubes: an efficient strategy to strengthen fibers. *American Chemical Society Nano*. 2010;**4**(1):312–316
- [52] Mylvaganam K, Zhang LC. Ballistic resistance capacity of carbon nanotubes. *Nanotechnology*. 2007;**18**(47):475701
- [53] Yakobson BI, Brabec CJ, Bernholc J. Nanomechanics of carbon tubes: instabilities beyond linear response. *Physical Review Letters*. 1996;**76**(14):2511–2514
- [54] Yu M-F, Dyer MJ, Chen J, Qian D, Liu WK, Ruoff RS. Locked twist in multiwalled carbon-nanotube ribbons. *Physical Review B*. 2001;**64**(24):241403
- [55] Liew KM, Wong CH, Tan MJ. Tensile and compressive properties of carbon nanotube bundles. *Acta Materialia*. 2006;**54**(1):225–231
- [56] Poncharal P, Wang ZL, Ugarte D, De Heer WA. Electrostatic deflections and electromechanical resonances of carbon nanotubes. *Science*. 1999;**283**(5407):1513–1516
- [57] Lourie O, Cox DM, Wagner HD. Buckling and collapse of embedded carbon nanotubes. *Physical Review Letters*. 1998;**81**(8):1638–1641
- [58] Arroyo M, Belytschko T. Nonlinear mechanical response and rippling of thick multiwalled carbon nanotubes. *Physical Review Letters*. 2003;**91**(21):215505
- [59] Liu JZ, Zheng Q, Jiang Q. Effect of bending instabilities on the measurements of mechanical properties of multiwalled carbon nanotubes. *Physical Review B*. 2003;**67**(7):075414
- [60] Qian D, Liu WK, Subramoney S, Ruoff RS. Effect of interlayer potential on mechanical deformation of multiwalled carbon nanotubes. *Journal of Nanoscience and Nanotechnology*. 2003;**3**:185–191



- [61] Kolmogorov AN, Crespi VH. Smoothest bearings: interlayer sliding in multiwalled carbon nanotubes. *Physical Review Letters*. 2000;**85**(22):4727–4730
- [62] Kolmogorov AN, Crespi VH. Registry-dependent interlayer potential for graphitic systems. *Physical Review B*. 2005;**71**(23):235415
- [63] Qian D, Liu WK, Ruoff RS. Load transfer mechanism in carbon nanotube ropes. *Composites Science and Technology*. 2003;**63**(11):1561–1569
- [64] Guo W, Zhong W, Dai Y, Li S. Coupled defect-size effects on interlayer friction in multiwalled carbon nanotubes. *Physical Review B*. 2005;**72**(7):075409
- [65] Zhang XH, Santoro GE, Tartaglino U, Tosatti E. Dynamical phenomena in fast sliding nanotube models. *Philosophical Magazine*. 2013;**93**(8):922–948
- [66] Yu M-F, Yakobson BI, Ruoff RS. Controlled sliding and pullout of nested shells in individual multiwalled carbon nanotubes. *Journal of Physical Chemistry B*. 2000;**104**(37):8764–8767
- [67] Cumings J, Zettl A. Low-friction nanoscale linear bearing realized from multiwall carbon nanotubes. *Science*. 2000;**289**(5479):602–604
- [68] Kis A, Jensen K, Aloni S, Mickelson W, Zettl A. Interlayer forces and ultralow sliding friction in multiwalled carbon nanotubes. *Physical Review Letters*. 2006;**97**(2):025501
- [69] Zhang R, Ning Z, Zhang Y, Zheng Q, Chen Q, Xie H, Zhang Q, Qian W, Wei F. Superlubricity in centimetres-long double-walled carbon nanotubes under ambient conditions. *Nature Nanotechnology*. 2013;**8**(12):912–916
- [70] Zheng Q, Jiang Q. Multiwalled carbon nanotubes as gigahertz oscillators. *Physical Review Letters*. 2002;**88**(4):045503
- [71] Guo W, Guo Y, Gao H, Zheng Q, Zhong W. Energy dissipation in gigahertz oscillators from multiwalled carbon nanotubes. *Physical Review Letters*. 2003;**91**(12):125501
- [72] Legoas SB, Coluci VR, Braga SF, Coura PZ, Dantas SO, Galvão DS. Molecular-dynamics simulations of carbon nanotubes as gigahertz oscillators. *Physical Review Letters*. 2003;**90**(5):055504
- [73] Zhao Y, Ma C-C, Chen G, Jiang Q. Energy dissipation mechanisms in carbon nanotube oscillators. *Physical Review Letters*. 2003;**91**(17):175504
- [74] Rivera JL, McCabe C, Cummings PT. Oscillatory behavior of double-walled nanotubes under extension: a simple nanoscale damped spring. *Nano Letters*. 2003;**3**(8):1001–1005
- [75] Liu P, Zhang YW, Lu C. Oscillatory behavior of gigahertz oscillators based on multiwalled carbon nanotubes. *Journal of Applied Physics*. 2005;**98**(1):014301
- [76] Zhao X, Cummings PT. Molecular dynamics study of carbon nanotube oscillators revisited. *Journal of Chemical Physics*. 2006;**124**(13):134705

- [77] Li B, Chang T. Tunable dual-frequency oscillators of carbon nanotubes. *Journal of Applied Physics*. 2010;**108**(5):054304
- [78] Fennimore AM, Yuzvinsky TD, Han W-Q, Fuhrer MS, Cumings J, Zettl A. Rotational actuators based on carbon nanotubes. *Nature*. 2003;**424**(6947):408–410
- [79] Zhang S, Liu WK, Ruoff RS. Atomistic simulations of double-walled carbon nanotubes (DWCNTs) as rotational bearings. *Nano Letters*. 2004;**4**(2):293–297
- [80] Servantie J, Gaspard P. Rotational dynamics and friction in double-walled carbon nanotubes. *Physical Review Letters*. 2006;**97**(18):186106
- [81] Cai K, Cai H, Yin H, Qin QH. Dynamic behavior of curved double-wall carbon nanotubes with rotating inner tube. *Royal Society of Chemistry Advances*. 2015;**5**(38):29908–29913
- [82] Cook EH, Buehler MJ, Spakovszky ZS. Mechanism of friction in rotating carbon nanotube bearings. *Journal of the Mechanics and Physics of Solids*. 2013;**61**(2):652–673
- [83] Tangney P, Cohen ML, Louie SG. Giant wave-drag enhancement of friction in sliding carbon nanotubes. *Physical Review Letters*. 2006;**97**(19):195901
- [84] Zhang XH, Santoro GE, Tartaglino U, Tosatti E. Dynamical chiral symmetry breaking in sliding nanotubes. *Physical Review Letters*. 2009;**102**(12):125502
- [85] Tangney P, Louie SG, Cohen ML. Dynamic sliding friction between concentric carbon nanotubes. *Physical Review Letters*. 2004;**93**(6):065503
- [86] Zhang X-H, Tartaglino U, Santoro GE, Tosatti E. Velocity plateaus and jumps in carbon nanotube sliding. *Surface Science*. 2007;**601**(18):3693–3696
- [87] Ajayan PM, Schadler LS, Giannaris C, Rubio A. Single-walled carbon nanotube polymer composites: strength and weakness. *Advanced Materials*. 2000;**12**(10):750–753
- [88] Bhushan B, Ling X, Jungen A, Hierold C. Adhesion and friction of a multiwalled carbon nanotube sliding against single-walled carbon nanotube. *Physical Review B*. 2008;**77**(16):165428
- [89] Bhushan B, Ling X. Adhesion and friction between individual carbon nanotubes measured using force-versus-distance curves in atomic force microscopy. *Physical Review B*. 2008;**78**(4):045429
- [90] Li C, Liu Y, Yao X, Ito M, Noguchi T, Zheng Q. Interfacial shear strengths between carbon nanotubes. *Nanotechnology*. 2010;**21**(11):115704
- [91] Salvétat J-P, Briggs GAD, Bonard J-M, Bacsá RR, Kulik AJ, Stöckli T, Burnham NA, Forró L. Elastic and shear moduli of single-walled Carbon nanotube ropes. *Physical Review Letters*. 1999;**82**(5):944–947
- [92] Kok ZKJ, Wong CH. Molecular dynamics simulation studies of mechanical properties of different carbon nanotube systems. *Molecular Simulation*. 2016;**42**(15):1274–1280

- [93] Huhtala M, Krasheninnikov AV, Aittoniemi J, Stuart SJ, Nordlund K, Kaski K. Improved mechanical load transfer between shells of multiwalled carbon nanotubes. *Physical Review B*. 2004;**70**(4):045404
- [94] Kis A, Csányi G, Salvétat J-P, Lee T-N, Couteau E, Kulik AJ, Benoit W, Brugger J, Forró L. Reinforcement of single-walled carbon nanotube bundles by intertube bridging. *Nature Materials*. 2004;**3**(3):153–157
- [95] Fonseca AF, Borders T, Baughman RH, Cho K. Load transfer between cross-linked walls of a carbon nanotube. *Physical Review B*. 2010;**81**(4):045429
- [96] Coleman JN, Khan U, Blau WJ, Gun'ko YK. Small but strong: a review of the mechanical properties of carbon nanotube-polymer composites. *Carbon*. 2006;**44**(9):1624–1652
- [97] Moniruzzaman M, Winey KI. Polymer nanocomposites containing carbon nanotubes. *Macromolecules*. 2006;**39**(16):5194–5205
- [98] Vigolo B, Pénicaud A, Coulon C, Sauder C, Pailler R, Journet C, Bernier P, Poulin P. Macroscopic fibers and ribbons of oriented carbon nanotubes. *Science*. 2000;**290**(5495):1331–1334
- [99] Dalton AB, Collins S, Muñoz E, Razal JM, Ebron VH, Ferraris JP, Coleman JN, Kim BG, Baughman RH. Super-tough carbon-nanotube fibres. *Nature*. 2003;**423**(6941):703–703
- [100] Ericson LM, Fan H, Peng H, Davis VA, Zhou W, Sulpizio J, Wang Y, Booker R, Vavro J, Guthy C, Parra-Vasquez ANG, Kim MJ, Ramesh S, Saini RK, Kittrell C, Lavin G, Schmidt H, Adams WW, Billups WE, Pasquali M, Hwang WF, Hauge RH, Fischer JE, Smalley RE. Macroscopic, neat, single-walled carbon nanotube fibers. *Science*. 2004;**305**(5689):1447–1450
- [101] Behabtu N, Young CC, Tsentalovich DE, Kleinerman O, Wang X, Ma AWK, Bengio EA, Ter Waarbeek RF, De Jong JJ, Hoogerwerf RE, Fairchild SB, Ferguson JB, Maruyama B, Kono J, Talmon Y, Cohen Y, Otto MJ, Pasquali M. Strong, light, multifunctional fibers of carbon nanotubes with ultrahigh conductivity. *Science*. 2013;**339**(6116):182–186
- [102] Zhu HW, Xu CL, Wu DH, Wei BQ, Vajtai R, Ajayan PM. Direct synthesis of long single-walled carbon nanotube strands. *Science*. 2002;**296**(5569):884–886
- [103] Li Y-L, Kinloch IA, Windle AH. Direct spinning of carbon nanotube fibers from chemical vapor deposition synthesis. *Science*. 2004;**304**(5668):276–278
- [104] Koziol K, Vilatela J, Moisala A, Motta M, Cunniff P, Sennett M, Windle A. High-performance carbon nanotube fiber. *Science*. 2007;**318**(5858):1892–1895
- [105] Ma W, Liu L, Zhang Z, Yang R, Liu G, Zhang T, An X, Yi X, Ren Y, Niu Z, Li J, Dong H, Zhou W, Ajayan PM, Xie S. High-strength composite fibers: realizing true potential of carbon nanotubes in polymer matrix through continuous reticulate architecture and molecular level couplings. *Nano Letters*. 2009;**9**(8):2855–2861

- [106] Jiang K, Li Q, Fan S. Spinning continuous carbon nanotube yarns. *Nature*. 2002;**419**(6909):801–801
- [107] Zhang M, Atkinson KR, Baughman RH. Multifunctional carbon nanotube yarns by downsizing an ancient technology. *Science*. 2004;**306**(5700):1358–1361
- [108] Li Q, Zhang X, DePaula RF, Zheng L, Zhao Y, Stan L, Holesinger TG, Arendt PN, Peterson DE, Zhu YT. Sustained growth of ultralong carbon nanotube arrays for fiber spinning. *Advanced Materials*. 2006;**18**(23):3160–3163
- [109] Zhao J, Zhang X, Pan Z, Li Q. Wide-range tunable dynamic property of carbon-nanotube-based fibers. *Advanced Materials Interfaces*. 2015;**2**(10):1500093
- [110] Hearle JWS, Hollick L, Wilson DK. *Yarn Texturing Technology*. Boca Raton: CRC Press; 2001
- [111] Zhao J, Zhang X, Di J, Xu G, Yang X, Liu X, Yong Z, Chen M, Li Q. Double-peak mechanical properties of carbon nanotube fibers. *Small*. 2010;**6**(22):2612–2617
- [112] Fang S, Zhang M, Zakhidov AA, Baughman RH. Structure and process-dependent properties of solid-state spun carbon nanotube yarns. *Journal of Physics: Condensed Matter*. 2010;**22**(33):334221
- [113] Miao M, McDonnell J, Vuckovic L, Hawkins SC. Poisson's ratio and porosity of carbon nanotube dry-spun yarns. *Carbon*. 2010;**48**:2802–2811
- [114] Liu H, Li S, Zhai J, Li H, Zheng Q, Jiang L, Zhu D. Self-assembly of large-scale micropatterns on aligned carbon nanotube films. *Angewandte Chemie International Edition*. 2004;**43**(9):1146–1149
- [115] Chakrapani N, Wei B, Carrillo A, Ajayan PM, Kane RS. Capillarity-driven assembly of two-dimensional cellular carbon nanotube foams. *Proceedings of the National Academy of Sciences*. 2004;**101**(12):4009–4012
- [116] Zhang X, Jiang K, Feng C, Liu P, Zhang L, Kong J, Zhang T, Li Q, Fan S. Spinning and processing continuous yarns from 4-inch wafer scale super-aligned carbon nanotube arrays. *Advanced Materials*. 2006;**18**(12):1505–1510
- [117] Liu K, Sun Y, Zhou R, Zhu H, Wang J, Liu L, Fan S, Jiang K. Carbon nanotube yarns with high tensile strength made by a twisting and shrinking method. *Nanotechnology*. 2010;**21**(4):045708
- [118] Li S, Zhang X, Zhao J, Meng F, Xu G, Yong Z, Jia J, Zhang Z, Li Q. Enhancement of carbon nanotube fibres using different solvents and polymers. *Composites Science and Technology*. 2012;**72**(12):1402–1407
- [119] Qiu J, Terrones J, Vilatela JJ, Vickers ME, Elliott JA, Windle AH. Liquid infiltration into carbon nanotube fibers: effect on structure and electrical properties. *American Chemical Society Nano*. 2013;**7**(10):8412–8422



- [120] in het Panhuis M, Maiti A, Dalton AB, van den Noort A, Coleman JN, McCarthy B, Blau WJ. Selective interaction in a polymer—single-wall carbon nanotube composite. *Journal of Physical Chemistry B*. 2003;**107**(2):478–482
- [121] Israelachvili JN. *Intermolecular and Surface Forces*. 2nd ed. San Diego: Academic Press; 1991.
- [122] Ryu S, Lee Y, Hwang J-W, Hong S, Kim C, Park TG, Lee H, Hong SH. High-strength carbon nanotube fibers fabricated by infiltration and curing of mussel-inspired catecholamine polymer. *Advanced Materials*. 2011;**23**(17):1971–1975
- [123] Ryu S, Chou JB, Lee K, Lee D, Hong SH, Zhao R, Lee H, Kim S-G. Direct insulation-to-conduction transformation of adhesive catecholamine for simultaneous increases of electrical conductivity and mechanical strength of CNT fibers. *Advanced Materials*. 2015;**27**(21):3250–3255
- [124] Liu K, Sun Y, Lin X, Zhou R, Wang J, Fan S, Jiang K. Scratch-resistant, highly conductive, and high-strength carbon nanotube-based composite yarns. *American Chemical Society Nano*. 2010;**4**(10):5827–5834
- [125] Naraghi M, Filleter T, Moravsky A, Locascio M, Loutfy RO, Espinosa HD. A multi-scale study of high performance double-walled nanotube-polymer fibers. *American Chemical Society Nano*. 2010;**4**(11):6463–6476
- [126] Zou J, Zhang X, Zhao J, Lei C, Zhao Y, Zhu Y, Li Q. Strengthening and toughening effects by strapping carbon nanotube cross-links with polymer molecules. *Composites Science and Technology*. 2016;**135**:123–127
- [127] Fang C, Zhao J, Jia J, Zhang Z, Zhang X, Li Q. Enhanced carbon nanotube fibers by polyimide. *Applied Physics Letters*. 2010;**97**(18):181906
- [128] Meng F, Zhang X, Li R, Zhao J, Xuan X, Wang X, Zou J, Li Q. Electro-induced mechanical and thermal responses of carbon nanotube fibers. *Advanced Materials*. 2014;**26**(16):2480–2485
- [129] Vilatela JJ, Elliott JA, Windle AH. A model for the strength of yarn-like carbon nanotube fibers. *American Chemical Society Nano*. 2011;**5**(3):1921–1927
- [130] Deng W-L, Qiu W, Li Q, Kang Y-L, Guo J-G, Li Y-L, Han S-S. Multi-scale experiments and interfacial mechanical modeling of carbon nanotube fiber. *Experimental Mechanics*. 2014;**54**(1):3–10
- [131] Jia J, Zhao J, Xu G, Di J, Yong Z, Tao Y, Fang C, Zhang Z, Zhang X, Zheng L, Li Q. A comparison of the mechanical properties of fibers spun from different carbon nanotubes. *Carbon*. 2011;**49**(4):1333–1339
- [132] Motta M, Moisala A, Kinloch IA, Windle AH. High performance fibres from ‘dog bone’ carbon nanotubes. *Advanced Materials*. 2007;**19**(21):3721–3726

- [133] Meng F, Zhao J, Ye Y, Zhang X, Li Q. Carbon nanotube fibers for electrochemical applications: effect of enhanced interfaces by an acid treatment. *Nanoscale*. 2012;**4**(23):7464–7468
- [134] Di J, Fang S, Moura FA, Galvão DS, Bykova J, Aliev A, de Andrade MJ, Lepró X, Li N, Haines C, Ovalle-Robles R, Qian D, Baughman RH. Strong, twist-stable carbon nanotube yarns and muscles by tension annealing at extreme temperatures. *Advanced Materials*. 2016;**28**(31):6598–6605
- [135] Wang Y, Li M, Gu Y, Zhang X, Wang S, Li Q, Zhang Z. Tuning carbon nanotube assembly for flexible, strong and conductive films. *Nanoscale*, 2015;**7**(7):3060–3066
- [136] Zhang L, Wang X, Xu W, Zhang Y, Li Q, Bradford PD, Zhu Y. Strong and conductive dry carbon nanotube films by microcombing. *Small*. 2015;**11**(31):3830–3836
- [137] Di J, Hu D, Chen H, Yong Z, Chen M, Feng Z, Zhu Y, Li Q. Ultrastrong, foldable, and highly conductive carbon nanotube film. *American Chemical Society Nano*. 2012;**6**(6):5457–5464
- [138] Liu W, Zhang X, Xu G, Bradford PD, Wang X, Zhao H, Zhang Y, Jia Q, Yuan F-G, Li Q, Qiu Y, Zhu Y. Producing superior composites by winding carbon nanotubes onto a mandrel under a poly(vinyl alcohol) spray. *Carbon*. 2011;**49**(14):4786–4791
- [139] Wang X, Yong ZZ, Li QW, Bradford PD, Liu W, Tucker DS, Cai W, Wang H, Yuan FG, Zhu YT. Ultrastrong, stiff and multifunctional carbon nanotube composites. *Materials Research Letters*. 2013;**1**(1):19–25
- [140] Cheng Q, Bao J, Park J, Liang Z, Zhang C, Wang B. High mechanical performance composite conductor: multi-walled carbon nanotube sheet/bismaleimide nanocomposites. *Advanced Functional Materials*. 2009;**19**(20):3219–3225
- [141] Cheng Q, Wang B, Zhang C, Liang Z. Functionalized carbon-nanotube sheet/bismaleimide nanocomposites: mechanical and electrical performance beyond carbon-fiber composites. *Small*. 2010;**6**(6):763–767
- [142] Jiang Q, Wang X, Zhu Y, Hui D, Qiu Y. Mechanical, electrical and thermal properties of aligned carbon nanotube/polyimide composites. *Composites Part B*. 2014;**56**:408–412
- [143] Han Y, Zhang X, Yu X, Zhao J, Li S, Liu F, Gao P, Zhang Y, Zhao T, Li Q. Bio-inspired aggregation control of carbon nanotubes for ultra-strong composites. *Scientific Reports*. 2015;**5**:11533
- [144] Wagner HD. Nanocomposites: paving the way to stronger materials. *Nature Nanotechnology*. 2007;**2**(12):742–744
- [145] Murayama T. Dynamic measurement of interfilament friction on staple yarns. *Journal of Applied Polymer Science*. 1979;**24**(6):1413–1417

- [146] Liu Q, Li M, Gu Y, Wang S, Zhang Y, Li Q, Gao L, Zhang Z. Interlocked CNT networks with high damping and storage modulus. *Carbon*. 2015;**86**:46–53
- [147] Guo W, Liu C, Zhao F, Sun X, Yang Z, Chen T, Chen X, Qiu L, Hu X, Peng H. A novel electromechanical actuation mechanism of a carbon nanotube fiber. *Advanced Materials*. 2012;**24**(39):5379–5384

IntechOpen

IntechOpen

